NASA TECHNICAL MEMORANDUM

NASA TM X-68162

NASA TM X-68162

FLIGHT AND WIND TUNNEL INVESTIGATION OF THE EFFECTS OF REYNOLDS NUMBER ON INSTALLED BOATTAIL DRAG AT SUBSONIC SPEEDS

by Roger Chamberlin and Bernard J. Blaha
Lewis Research Center
Cleveland, Ohio

TECHNICAL PAPER proposed for presentation at
Eleventh Aerospace Sciences Meeting and Technical Display
sponsored by the American Institute of Aeronautics and Astronautics
Washington, D.C., January 10-12, 1973

FLIGHT AND WIND TUNNEL INVESTIGATION OF THE EFFECTS OF REYNOLDS NUMBER ON INSTALLED BOATTAIL DRAG AT SUBSONIC SPEEDS

Roger Chamberlin and Bernard J. Blaha

Lewis Research Center
National Aeronautics and Space Administration
Cleveland, Ohio

Abstract

A flight and wind tunnel investigation was conducted to determine the effects of Reynolds number on the installed boattail drag of an underwing nacelle. Tests were run on a modified F-106B aircraft and 0.05 and 0.22 scale wind tunnel models. Tests were conducted at Mach numbers of 0.6 and 0.9 and over a 16 to 1 range of Reynolds numbers. Highest drag was obtained at intermediate Reynolds numbers corresponding to about the lowest flight values and that of the 0.22 scale model. Significantly lower drag was obtained at both higher and lower Reynolds numbers.

Introduction

E-7221

An occurrence that is still happening too frequently in the development of present generation aircraft is to discover that in-flight performance does not agree with extrapolated wind test results.[1-3] The most probable reason for this is that wind tunnel tests are conducted at Reynolds numbers considerably lower than flight values. There are no wind tunnel facilities presently available for full scale, high speed model testing, so small subscale model results must be used.

Many new multimission military aircraft are utilizing turbofan engines. The turbofan engine has a lower specific fuel consumption than the turbojet engine resulting in an increase in aircraft range, expecially at subsonic cruise. However, it does necessitate a large nacelle and in the subsonic cruise condition with the primary nozzle closed there is a large boattail area. The aft end drag for an aircraft with this engine can be a high percentage of the total aircraft drag.

Flight tests made at the Lewis Research Center on boattailed nozzles suitable for use with turbofan engines showed that Reynolds number had a significant effect on boattail drag.[4] This study was continued both in flight and with two wind tunnel models. The flight test phase of this program utilizes a modified F-106B, which has been modified to carry two aft-mounted underwing nacelles housing J85 afterburning turbojet engines. Three different high-angle boattail geometries, typical of those currently used for turbofan powered aircraft with supersonic dash capability, were tested. Wind tunnel tests in the 8 by 6 Foot Supersonic Wind Tunnel were conducted at low Reynolds numbers with a 0.05 scale F-106 full-span model, and at intermediate Reynolds numbers with a 0.22 scale half-span model. The 0.05 scale model was tested with solid nacelles that had jet boundary simulators. The 0.22 scale model was tested both with a turbojet engine simulator and a second configuration with the nacelle inlet closed off and a solid jet boundary simulator. Data were obtained at Mach numbers of 0.6 and 0.9. Each model gave data at a particular Reynolds number and the aircraft was flown over a range of Reynolds numbers at both Mach numbers. A 16 to 1 total range in Reynolds number was achieved.

Flight Program

An F-106B (two seat) aircraft was modified to carry two J85 afterburning engines as shown in Fig. 1. Cutouts were made in the elevons, the two underwing nacelles were attached, and a fuel system was added in the missile bay. A digital data system was installed along with scannervalves which sample pressure orifices. The system permitted the boattails to be instrumented with 90 static pressures. The boattail statics were area weighted in ten rows and all the drag data are from pressure integration. Details of the other aircraft modifications are given in Refs. 5 and 6, and details of the instrumentation system and electronics are given in Ref. 7. A schematic of the research nacelle with the boattail nozzle is shown in Fig. 2. The nacelles were located at the 32 percent semispan with 0° cant and a downward incidence of $4\frac{1}{2}^{\circ}$ (relative to the wing chord line) so the aft portion of the nacelle was tangent to the aft wing lower surface. Details of the wing modifications, nacelle shape, and mounting strut are given in Ref. 5. The gas generator for the nozzle was a J85-13 turbojet engine with afterburner. In order to achieve the ratio of nacelle cross-sectional area to nozzle exit area similar to a turbofan engine installation, the internal area of the nozzles had to be quite small. Because of this small nozzle exit area the variable-area primary nozzle on the J85 was locked at approximately 709.7 cm^2 (110 $in.^2$) permitting operation only at military power and below.

The aircraft was flown over a range of Reynolds number at both Mach 0.6 and 0.9. The Reynolds number was varied by changing altitude. In order to hold Mach number and angle-of-attack constant the data were taken in coordinated turns. By flying in turns at varying load factors, Reynolds number was varied from 23×10^6 [3048 m (10 000 ft) altitude] to 57×10^6 [9144 m (30 000 ft)] at Mach 0.6, and at Mach 0.9 from 23×10^6 [4572 m (15 000 ft)] to 65×10^6 [13 716 m (45 000 ft)]. The Reynolds number was based on a characteristic length of 5.18 m (17 ft), which takes into consideration the wing chord at this station (approximately 7.32 m (24 ft)), and the nacelle length (approximately 3.96 m (13 ft)). At each Mach number the angle-of-attack was constant over the range of altitude.

Tufts were mounted on the top of the boattails and movies were taken with a camera mounted in the tail. The camera was activated by the data system and ran only during the 11.6 second data scan periods. The films were used to observe the flow patterns and detect the presence of separation.

Wind Tunnel Program

Both of the subscale models were tested in the

8- by 6-Foot Supersonic Wind Tunnel. The 0.22 scale model was a half-span F-106 model mounted on a reflection plate (fig. 3). This model was tested with a turbojet engine simulator and also with a conical forebody closing the nacelle inlet and a solid jet boundary simulator mounted on the nozzle (fig. 4). The engine simulator incorporated a six-stage, axial flow compressor powered by a three-stage, axial-flow turbine. High pressure warm air was used to drive the turbine and it was possible to match the inlet mass flow ratio and the pressure ratio of the J85 engine at military power with the same area ratio (A^*/A_{max}). Details of the turbojet simulator and its operating characteristics are given in Ref. 8. The design characteristics of this simulator permit independent operation over a wide range of both inlet mass flow ratios and nozzle pressure ratios which equal those in flight. By injecting makeup air, nozzle pressure ratio can be varied independent of inlet mass flow ratio, or inlet mass flow can be varied at a constant nozzle pressure ratio.

The 0.05 scale model was a sting-mounted full-span model (fig. 5). For these tests the nacelles were closed with conical forebodies (not shown in fig. 5) and solid jet boundary simulators were used. Both model nozzles had four rows of eight area-weighted static pressures along the boattail. The boattail drags for both the models and the aircraft were obtained by pressure integration. On the 0.22-scale model data were obtained at a Reynolds number of 14.5×10^6 at Mach 0.6 and a Reynolds number of 18×10^6 at Mach 0.9. Data on this model were taken at angles-of-attack of 3° and 7°. On the 0.05-scale model data were obtained at a Reynolds number of 3.5×10^6 at Mach 0.6 and a Reynolds number of 4×10^6 at Mach 0.9. On this model it was possible to investigate a range of angle-of-attack from 0° to 15°. These Reynolds numbers are based on a characteristic length which is the appropriate scale of the flight characteristic length.

Three different high-angle boattail geometries were tested on the aircraft and on the two models (fig. 6). The nozzles are designated by a four-digit number. The first two numbers correspond to the radius ratio, R/R_c, multiplied by 100 and the second two numbers correspond to the terminal boattail angle. Thus nozzle 2524 has a radius ratio R/R_c of 0.25, and has a terminal boattail angle of 24°. The radius ratio R/R_c is defined as the ratio of the radius of the boattail shoulder to the radius of a complete circular arc nozzle, with the same boattail angle and ratio of nozzle exit area to nacelle area. This numbering system will be used throughout the remainder of this paper. Two of the nozzles had 24° terminal angles and one had a 16° terminal angle. These nozzles were part circular arc transitioning into a conic section on the aft portion. Detailed dimensions of the external contours are given in Fig. 7. The boattail projected area was equal to 75 percent of the nacelle projected area.

Results

The flow pattern and pressure distribution around high-angle boattail nozzles is illustrated in Fig. 8 for high subsonic flight speeds. As the flow approaches the boattail shoulder, the pressure is slightly less than freestream because of the presence of the wing and the nacelle upstream of this point. As the flow traverses the boattail shoulder it overexpands. If the radius of the shoulder is small, the overexpansion can be large. Just downstream of the shoulder a recompression begins, and if the flow is attached, it recompresses along the remaining length of the boattail. At the end of the boattail the flow has generally recompressed to a value greater than the freestream static pressure. This recompression region presents an adverse pressure gradient to the local boattail boundary layer. If the flow separates, the point of separation on these nozzles is generally downstream of the shoulder and there is a loss of recompression causing an increase in the drag.

Figure 9 shows the effect of Reynolds number on boattail drag coefficient at both Mach 0.6 and 0.9. As can be seen the drag coefficient was maximum at a value near the low end of the flight Reynolds number range and dropped off as Reynolds number was either raised or lowered. First consider the portion of the curves that begins at the peak and drops off as Reynolds number is increased. The reduction in drag was primarily caused by a reduction in the amount of separation on the boattail. This can be seen by examining the two flight pressure distribution trends shown in Fig. 10. Nozzle 2516 which was a 16° boattail angle, had little separation at any condition and showed little change in drag over this range of Reynolds number variation. The other two nozzles, however, were 24° boattails and incurred significant areas of separated flow. The pressures on these nozzles showed a marked effect from separation changes. Separation was not always evident from the pressure distributions alone, as will be shown later, so the tuft films were helpful for detecting separation and resulting flow patterns.

As the Reynolds number was increased in this range, the boundary layer became thinner. With a thinner turbulent boundary layer the flow will generally penetrate an adverse pressure gradient farther without separating. Only a minute change in separation axial location results in a significant change in pressure level due to the sharp pressure rise downstream of the boattail shoulder. So by increasing the Reynolds number in this range the separation was delayed to a point farther downstream on the boattail. As the separation was reduced more recompression was gained (fig. 10(b) through through 10(f)) resulting in lower drag.

In addition to this simple concept of attached flow-separated flow there was a dynamic phenomena included. There were many cases where the boattail pressures were not representative of either the obviously attached flow (smooth recompression) or obviously separated flow (flat cutoff in recovery). Many of the pressure distributions fell between these two limits. One possible explanation is that the flow was oscillating between attached and separated. The pressures measured were time-averaged by the instrumentation so they reflected a combination of the two actual conditions. When this situation was present, the tufts on the boattail lay flat pointing in the streamwise direction; however, they still exhibited some movement of oscillations. At high Reynolds numbers the pressures were more nearly the value of attached flow and the tufts moved less; at low Reynolds numbers the pressures tended more toward a separated case and the tuft movement increased. The two types of separation usually occurred simultaneously at different circumferential regions of the boattail, and each local

region varied with changes in Reynolds number. The net result at this end of the Reynolds number range was a reduction in boattail drag with increasing Reynolds number.

Now consider the portion of the curve that begins at the peak and drops off as Reynolds number is decreased. The reduction in drag in this range was primarily associated with a reduction of the overexpansion at the boattail shoulder. This can be seen by examining the pressure curves in Fig. 10 again, including the curves from the two models. In general at the lower Reynolds numbers the minimum pressure at the shoulder increased resulting in lowered boattail drag. This effect has been observed previously on isolated nozzle tests.[9] As the boundary layer becomes thicker (lower Reynolds numbers) it softens the turn the flow makes at the shoulder. The boundary layer effectively increases the radius at the shoulder so the flow doesn't experience as sharp a turn, accelerates less and the pressures near the shoulder are therefore higher.

This can be seen on nozzle 2516 which had very little separation and also on nozzle 6524 which had a limited amount of separated flow. On nozzle 2524 there was a great deal of separation which continued to move upstream with lower Reynolds numbers. Again there was a reduction in the overexpansion at the shoulder, eliminating almost all the overexpansion. This nearly eliminated the turn at the shoulder so the pressures remained near freestream static. There was still a small recompression on the aft boattail, but the recompression began at a much higher pressure. The aft boattail pressures recompressed to high values, yielding a larger decrease in drag then seen on the other two nozzles.

Figure 11 shows a comparison of indicated separation from tufts and pressure distributions. The pressure curves shown are four rows on the upper portion of the nozzle. The tufts were mounted on the nozzle between the rows of pressure orifices. The tuft picture is one frame from the high-speed movie film. An initial examination of the pressure curves alone shows they are similar, and none is obviously representative of a typical separated or attached flow. If a choice were to be made one might say they were all attached flows. However, examining the tuft picture shows the last three tufts on the A and B rows indicated separated flow, while the other two rows indicated attached flow (there is a fourth row of tufts that is difficult to see in the photograph). A closer examination of the pressure curves will reveal small differences in level and shape of the No. 1 and 2 pressure rows which correspond to the separated condition. However, these differences are so small that they could not be used alone to predict separation. Much of the data recorded on the flight tests was similar to this. One explanation for this is that the flow was unsteady and oscillated between attached and separated as discussed previously. The pressures are time averaged so that this type of oscillation produces values that are intermediate between those of the two flow conditions. More recent unpublished dynamic boundary-layer data on nozzle 2524 has verified that the oscillations were occurring. Random oscillations at frequencies below 100 Hz were detected in flight with a dynamic boundary layer rake mounted near the end of the boattail.

The 0.22 scale model was run with both a turbojet engine simulator and with the nacelle inlets closed off and included jet boundary simulators. (This latter configuration duplicated the nacelle geometry used for the 0.05 scale model.) A comparison of these two operating conditions is shown in Fig. 12, where boattail drag variation with nozzle pressure ratio is shown. The jet boundary simulator data are plotted at the design pressure ratio for these nozzles ($p_e/p_0 = 1.0$). Very good agreement is seen between the two for all three nozzles, for conditions presented here. Therefore the 0.05 scale data is valid for showing a Reynolds number effect and is not the result of using a closed inlet and solid jet boundary simulator. It has been shown[10] that closing off the nacelle with a conical forebody has a negligible effect on boattail drag at subsonic speeds. Also, from Fig. 12, the effect of nozzle pressure ratio on boattail drag is relatively small for the range of nozzle pressure ratio investigated.

The effect of angle-of-attack on boattail drag is shown in Fig. 13 for the 0.05-scale model. Angle-of-attack had very little effect on the boattail drag at Mach 0.6, but did have a significant effect at high angles (8° and above), at Mach 0.9. At Mach 0.9 the flight angle-of-attack range was lower where the effects are small. Most of the Mach 0.9 data shown here were at the same angle-of-attack for flight and wind tunnel.

To summarize, it has been found that Reynolds number can significantly affect installed boattail drag coefficient. This result is shown again in Fig. 14 along with schematics of the pressure distributions at the three regions of the drag curve. The apparent effects seen on the boattail pressures generate an understanding of the basic phenomena which resulted in the unusual shape seen for the drag curve. At very low Reynolds numbers (0.05-scale model) there is very little overexpansion at the boattail shoulder, most probably due to the very thick boundary layer. At these low Reynolds numbers the separation point is closest to the boattail shoulder. However, since the pressures are not low at the shoulder only a small recompression is required to minimize the drag. Therefore the separation does not result in a severe penalty.

As the Reynolds number is increased (0.22 scale and low flight values) the boundary layer thins and there is more overexpansion at the shoulder. This overexpansion requires a significant recompression to maintain low drag; but the separation point is still relatively close to the shoulder and prevents the recompression. At this condition the separation combined with the large overexpansion at the shoulder is a severe penalty resulting in maximum drag.

As the Reynolds number is increased still further (to high flight values) the boundary layer thins even more. The overexpansion at the shoulder remains essentially the same, but the separation point moves aft on the boattail. At the highest Reynolds number values there is very little separation left and the flow recompresses generally to values above freestream static. Because the separation is now gone the drag values are again relatively low.

Conclusions

A series of wind tunnel and flight tests have been conducted to determine the effect of Reynolds number on the installed boattail drag at subsonic

speeds. The high-angle boattail nozzles tested were subsonic cruise configurations of nozzles designed for turbofan-powered aircraft with supersonic dash capability. Flight data are compared with 0.22-scale and 0.05-scale model data. The following results were obtained.

1. Highest drag was obtained at intermediate Reynolds numbers corresponding to about the lowest flight values and that of the 0.22-scale model. Significantly lower drag was obtained at both higher and lower Reynolds numbers.

2. Changes in Reynolds number had two effects on the boattail pressures. The amount of overexpansion at the boattail shoulder was significantly reduced at very low wind tunnel Reynolds numbers, resulting in low drag. At higher flight values, increasing the Reynolds number reduced the amount of separation and increased the recompression on the aft portion of the boattail, lowering the drag.

3. Separation cannot always be detected with static pressure distributions alone.

4. Boattail drag data obtained in the wind tunnel with a solid jet boundary simulator agreed well with data using a turbojet engine simulator at the design pressure ratio.

5. Boattail drag is relatively insensitive to angle-of-attack changes at Mach 0.6. At Mach 0.9 there is no effect until an angle-of-attack of approximately 8° and then the boattail drag increases with angle-of-attack.

Symbols

A_{max}	nacelle area at boattail juncture
A^*	nozzle geometric throat area
C_D	boattail pressure drag coefficient
C_p	pressure coefficient, $p-p_0/0.7\ p_0M_0^2$
d	nacelle diameter at boattail juncture
ℓ	nozzle length
M_0	free-stream Mach number
P	total pressure at nozzle throat
p	boattail static pressure
p_e	static pressure nozzle exit
p_0	free-stream static pressure
R	radius at nozzle boattail shoulder
R_c	radius of a complete circular arc boattail with a fixed exit to nacelle area ratio and a fixed terminal boattail angle
R_e	Reynolds number--based on a characteristic length of 5.18 m (17 ft) for flight and appropriately scaled values for the wind tunnel models
X	axial distance from boattail shoulder to the point where the boattail contour becomes a conic section
x	axial distance from beginning of boattail shoulder
Y	diameter at the nozzle exit
Z	length of solid jet boundary simulator
α	angle-of-attack
β	terminal boattail angle

References

1. Blackwell, J. A. Jr., "Preliminary Study of Effects of Reynolds Number and Boundary-Layer Transition Location on Shock-Induced Separation," TN D-5003, 1969, NASA, Hampton, Va.

2. Loving, D. L., "Wind-Tunnel—Flight Correlation of Shock-Induced Separated Flow," TN D-3580, 1966, NASA, Hampton, Va.

3. Saltzman, E. J. and Bellman, D. R., "A Comparison of Some Aerodynamic Drag Factors as Determined in Full-Scale Flight With Wind-Tunnel and Theoretical Results," TM X-67413, 1971, NASA, Edwards, Calif.

4. Chamberlin, R., "Flight Investigation of 24° Boattail Nozzle Drag at Varying Subsonic Flight Conditions," TM X-2626, 1972, NASA, Cleveland, Ohio.

5. Crabs, C. C., Mikkelson, D. C., and Boyer, E. O. "An Inflight Investigation of Airframe Effects on Propulsion System Performance at Transonic Speeds," presented at the 13th Annual Symposium of the Society of Experimental Test Pilots, Los Angeles, Calif., Sept. 25-27, 1969.

6. Mikkelson, D. C. and Head, V. L., "Flight Investigation of Airframe Installation Effects on a Variable Flap Ejector Nozzle of an Underwing Nacelle at Mach Numbers from 0.5 to 1.3," TM X-2010, 1970, NASA, Cleveland, Ohio.

7. Groth, H. W., Samanich, N. E., and Blumenthal, P. A., "Inflight Thrust Measuring System for Underwing Nacelles Installed on a Modified F-106 Aircraft," TM X-2356, 1971, NASA, Cleveland, Ohio.

8. Steffen, F. W., Satmary, E. A., Vance, M. R., and Nosek, S. M., "A Turbojet Simulator for Mach Numbers up to 2.0," TM X-67973, 1972, NASA, Cleveland, Ohio.

9. Blaha, B. J. and Bresnahan, D. L., "Wind Tunnel Installation Effects on Isolated Afterbodies at Mach Numbers from 0.56 to 1.5. TM X-52581, 1969, NASA, Cleveland, Ohio.

10. Blaha, B. J. and Mikkelson, D. C., "Wind Tunnel Investigation of Airframe Installation Effects on Underwing Engine Nacelles at Mach Numbers From 0.56 to 1.46," TM X-1683, 1968, NASA, Cleveland, Ohio.

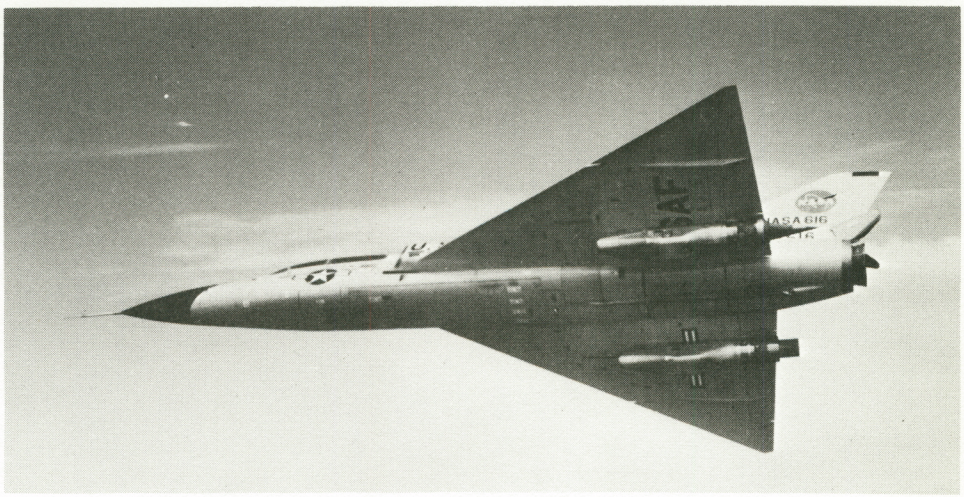

C-69-2871

Figure 1. - Modified F-106B in flight.

E-7221

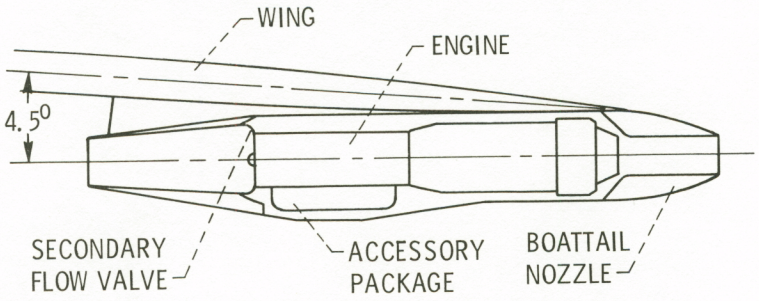

Figure 2. - Nacelle-engine installation.

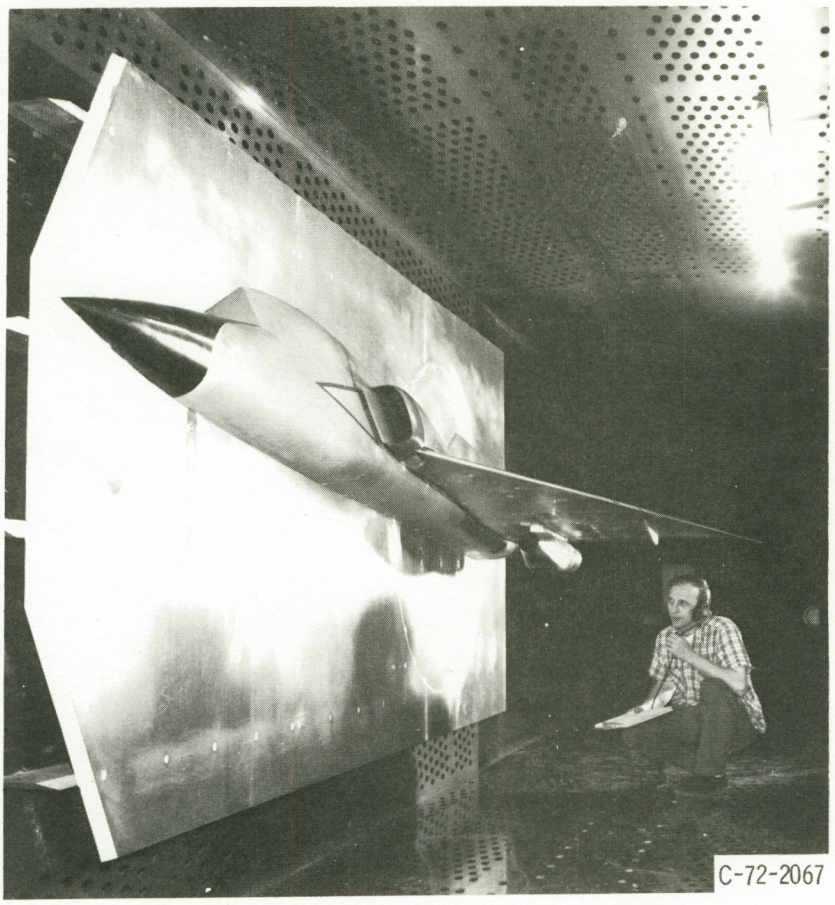

Figure 3. - 0.22 scale F-106 model in 8x6 tunnel.

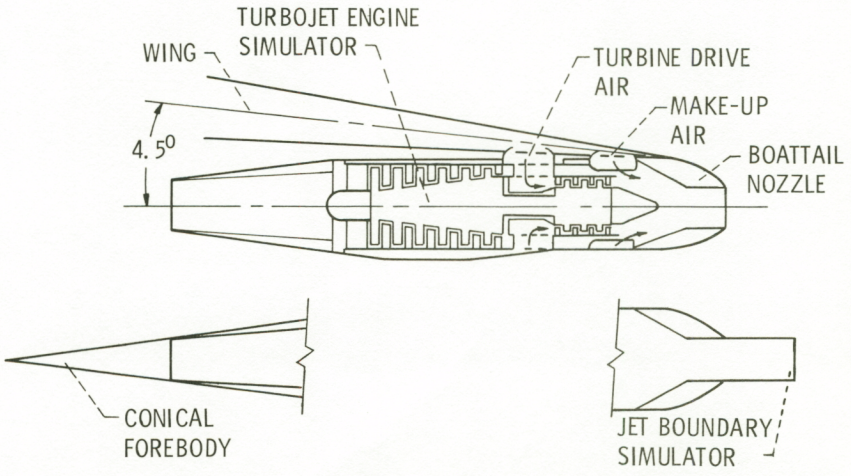

Figure 4. - 0.22 Scale model turbojet simulator and nacelle installation.

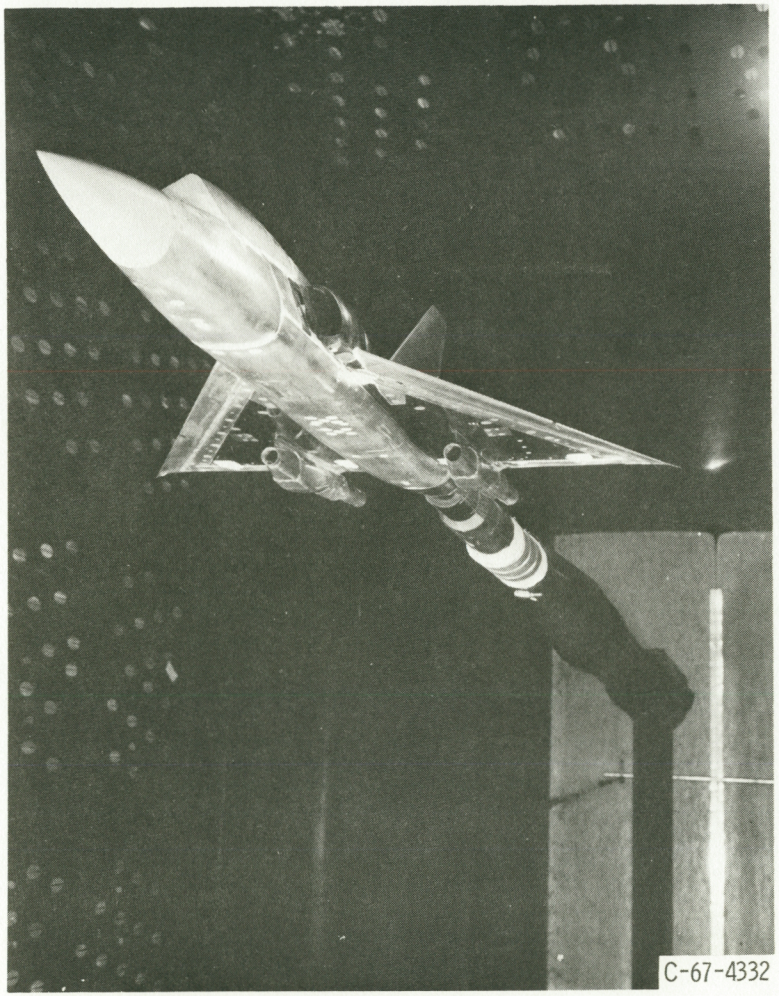

Figure 5. - 0.05 scale F-106 model in 8x6 tunnel.

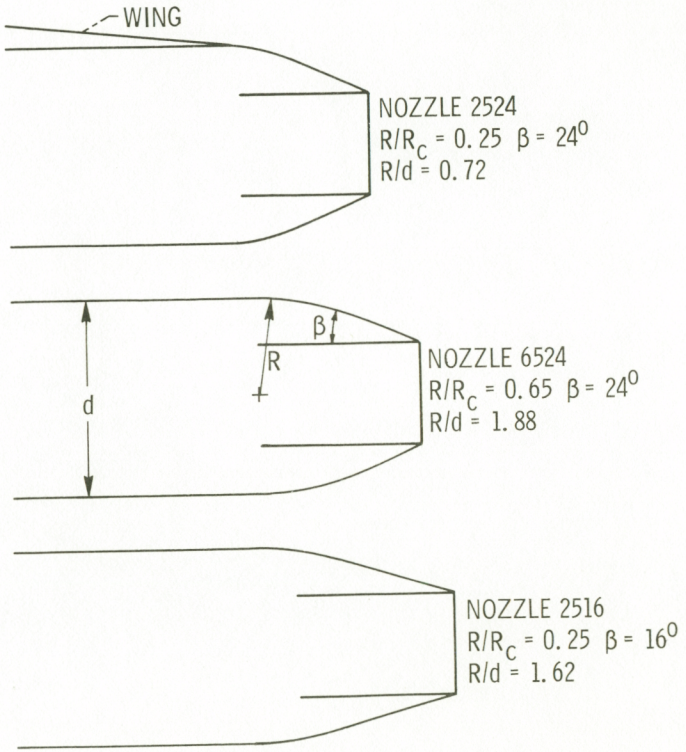

Figure 6. - Comparison of nozzle geometries tested.

	NOZZLE 2524	NOZZLE 6524	NOZZLE 2516
β	24°	24°	16°
X/d	0.50	0.50	0.50
Y/d	0.29	0.76	0.44
l/d	0.71	0.96	1.10
R/d	0.72	1.88	1.61
JET BOUNDARY SIMULATOR Z/d	0.22 SCALE 1.82	0.05 SCALE 2.42	

d - NACELLE DIAMETER AT BOATTAIL JUNCTURE
FLIGHT NOZZLES - 63.50 (25.00)
0.22 SCALE - 13.97 (5.50)
0.05 SCALE - 3.15 (1.24)

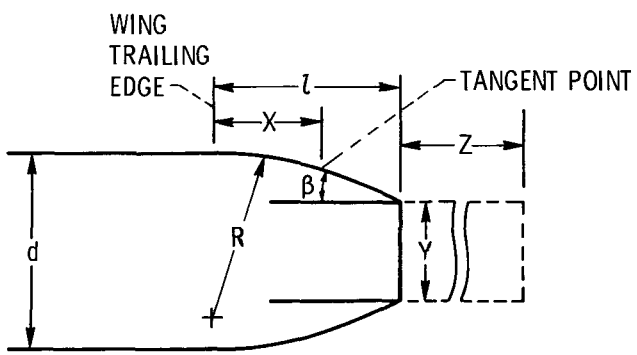

Figure 7. - Boattail nozzle dimensions. (Dimensions are in centimeters (in.).)

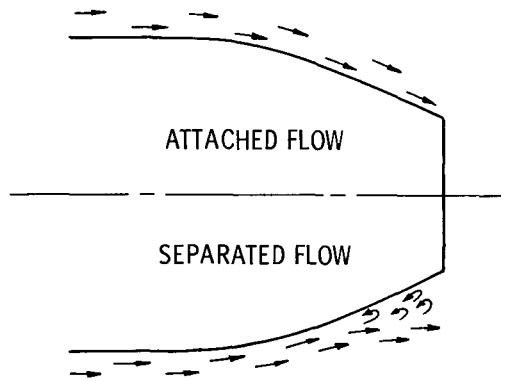

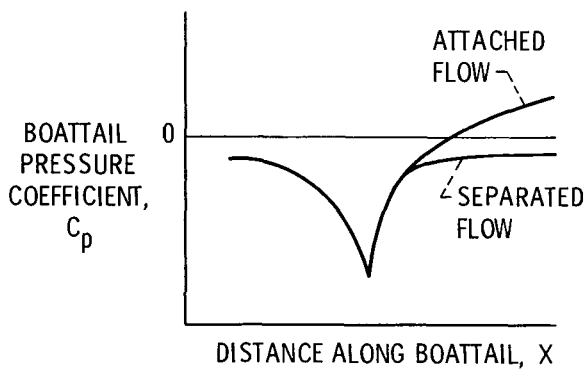

Figure 8. - Typical boattail flows.

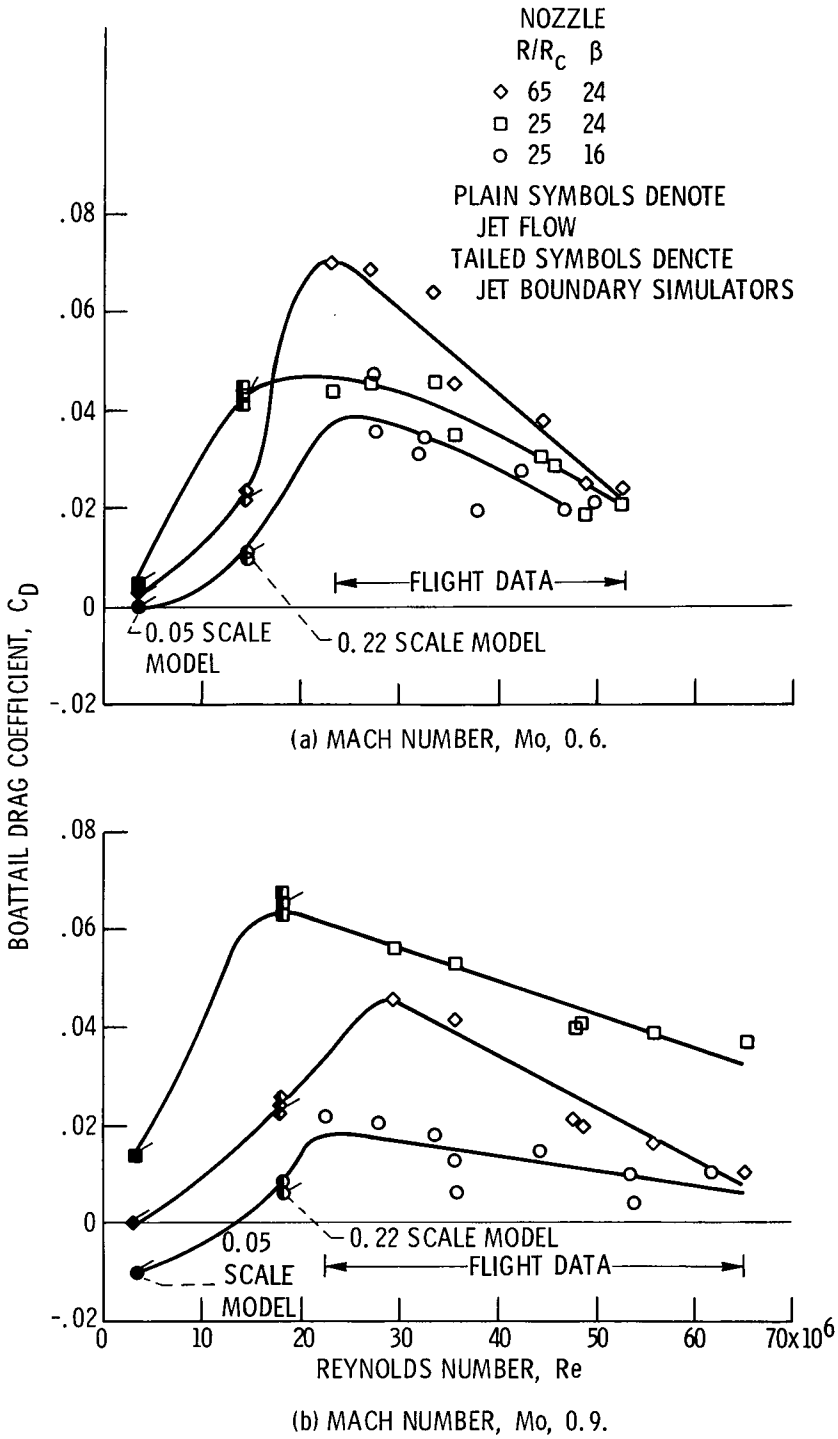

(a) MACH NUMBER, Mo, 0.6.

(b) MACH NUMBER, Mo, 0.9.

Figure 9. - Effect of Reynolds number on boattail drag coefficient.

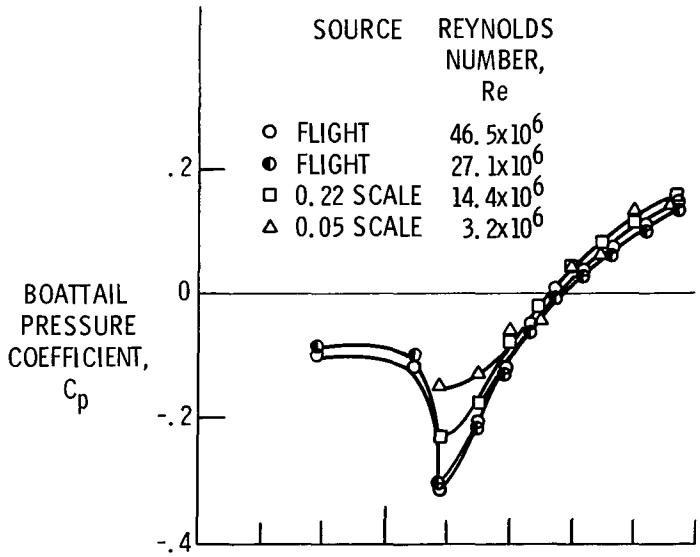

(a) NOZZLE 2516, Mo = 0.6.

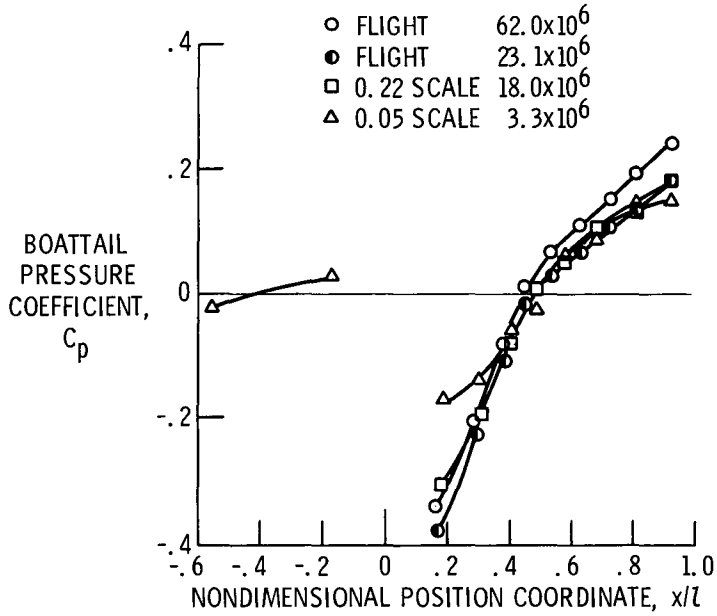

(b) NOZZLE 2516, Mo = 0.9.

Figure 10. - Effect of Reynolds number on boattail pressure distribution.

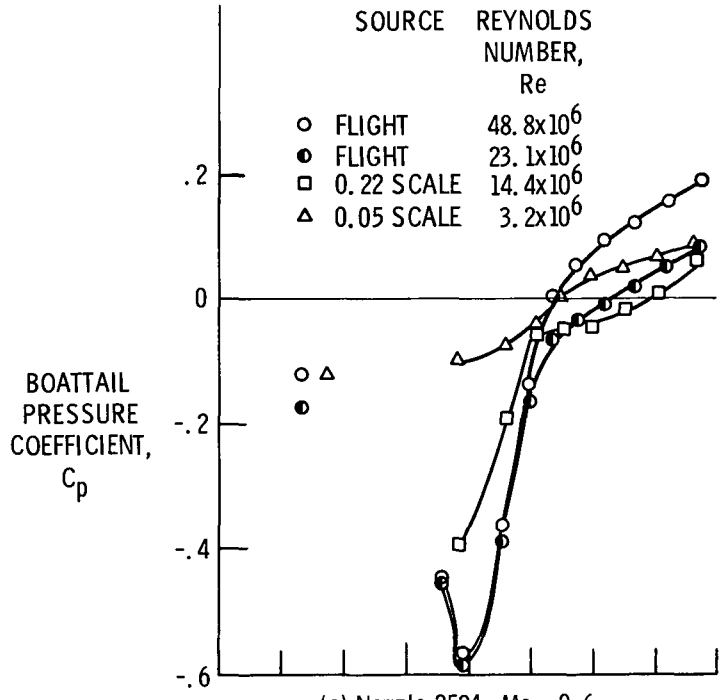

(c) Nozzle 2524, Mo = 0.6.

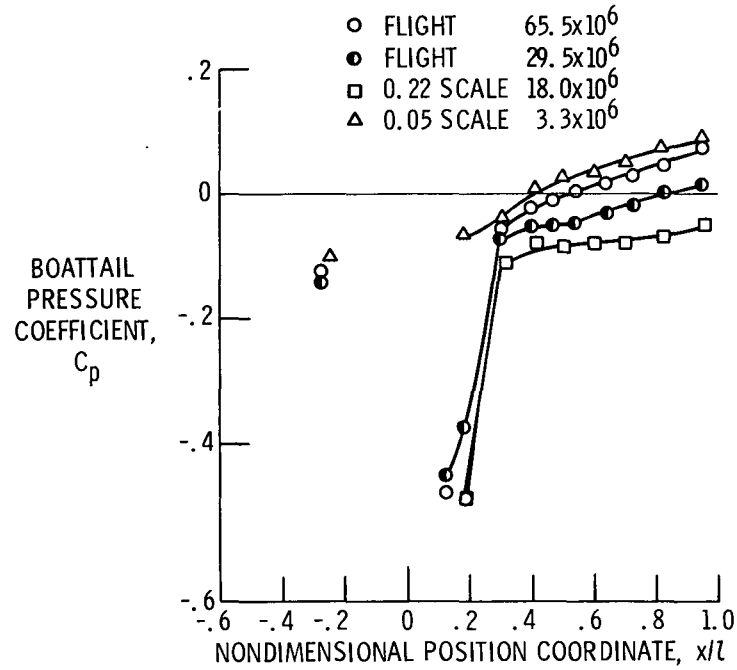

(d) NOZZLE 2524, Mo = 0.9.

Figure 10. - Continued.

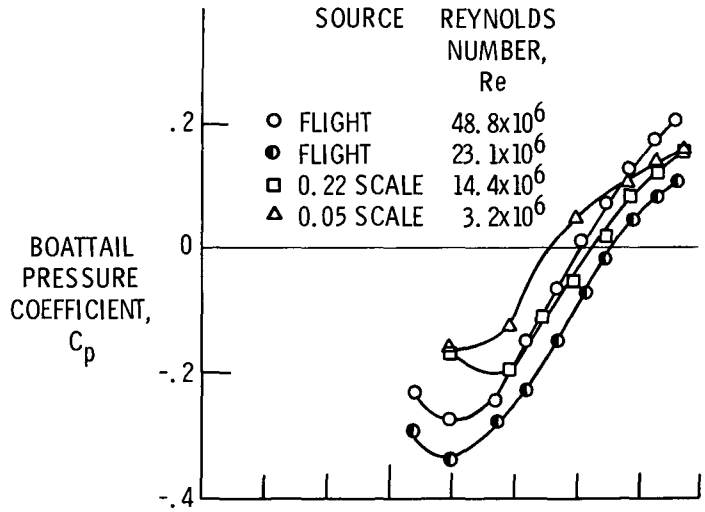

(e) NOZZLE 6524, Mo = 0.6.

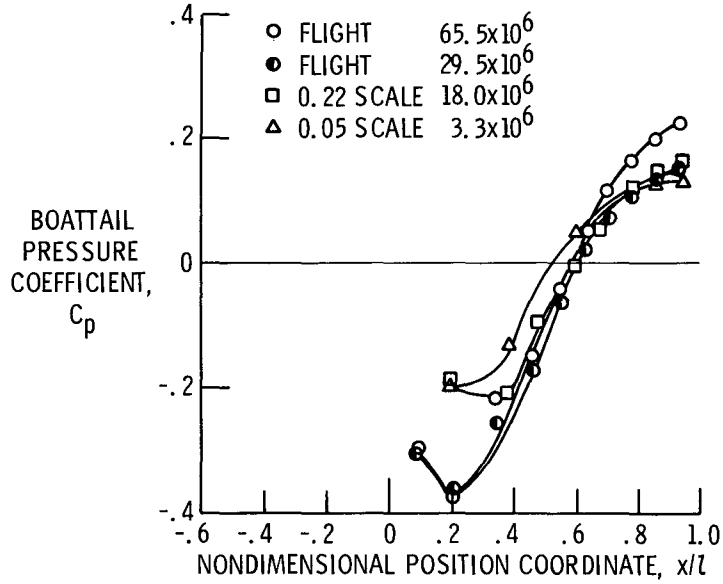

(f) NOZZLE 6524, Mo = 0.9.

Figure 10. - Concluded.

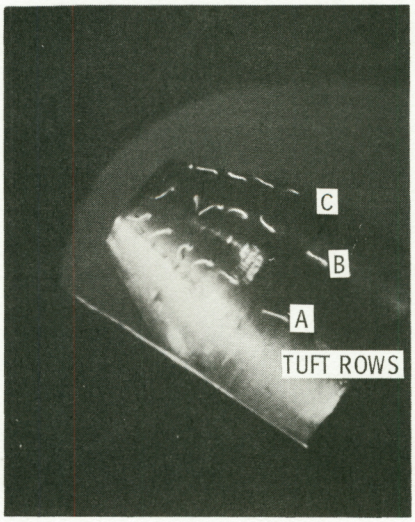

(a) TUFT PICTURE.

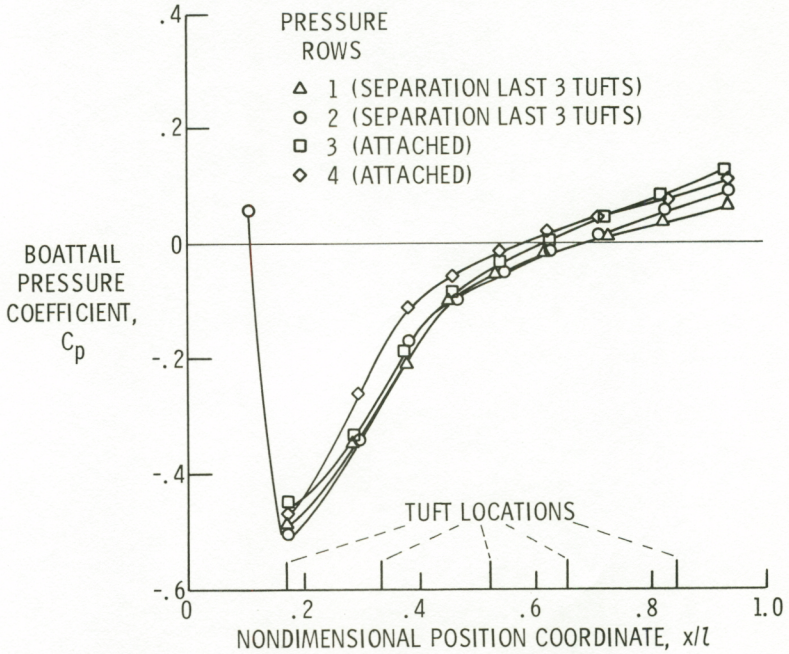

(b) PRESSURE DISTRIBUTION.

Figure 11. - Determination of separation. Nozzle 2524; Mo, 0.9; Re, 49.2×10^6.

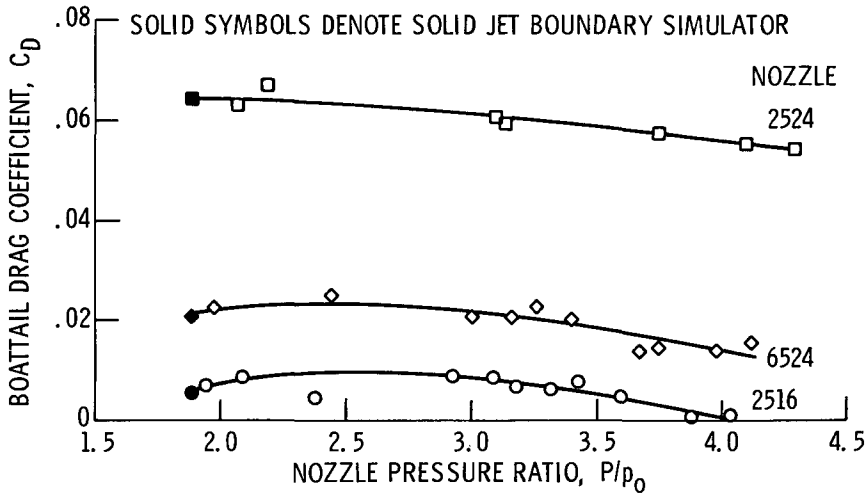

Figure 12. - Effect of pressure ratio on boattail drag coefficient on the 0.22 scale model; Mo, 0.9; Re, 18.0×10^6.

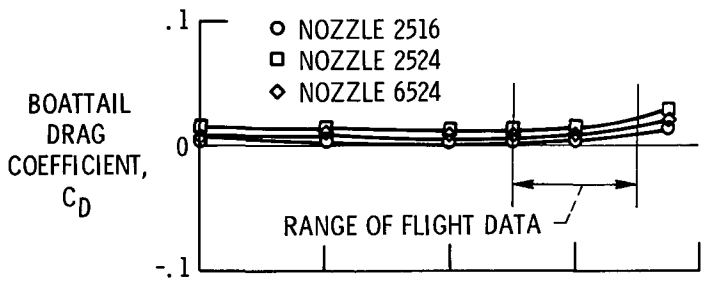

(a) FREE-STREAM MACH NUMBER, Mo, 0.6.

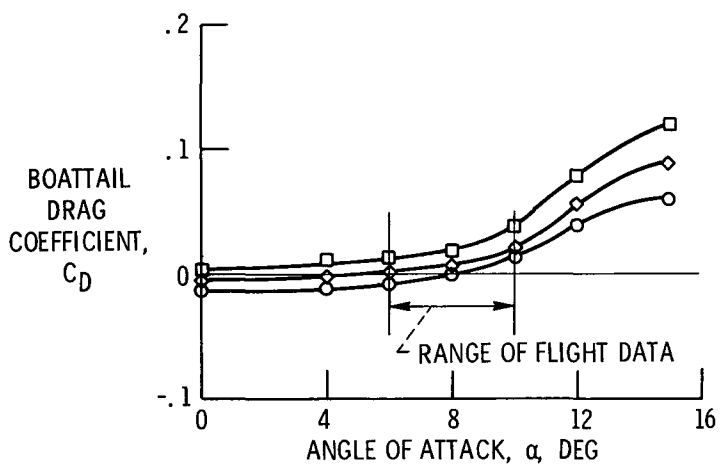

(b) FREE STREAM MACH NUMBER, Mo, 0.9.

Figure 13. - Effect of angle of attack on boattail drag coefficient with the 0.05 scale model.

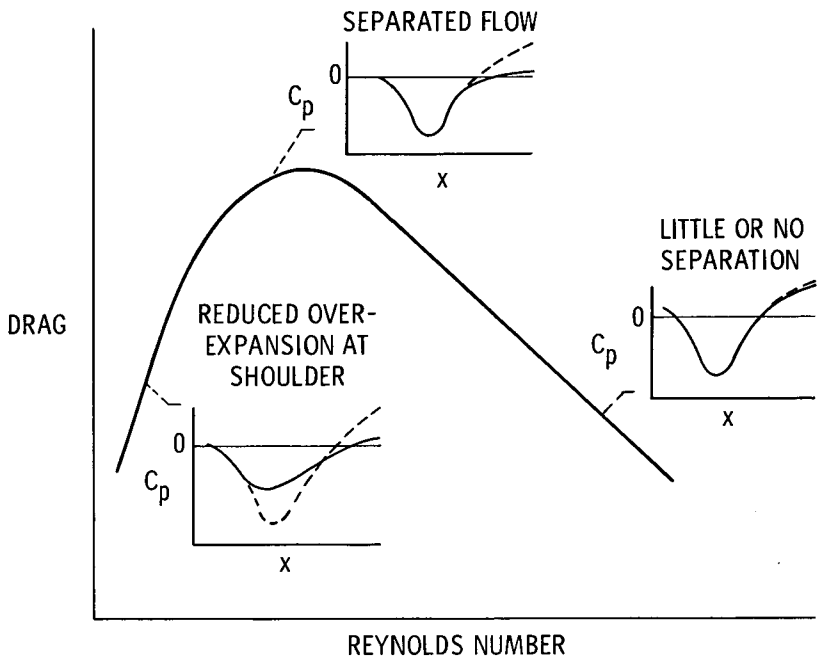

Figure 14. - Summary of Reynolds number effects.